Title

Macular SD-OCT Outcome Measures: Comparison of Local Structure-Function Relationships and Dynamic RangeComparative Utility of Macular SD-OCT Measures

Journal

Investigative Ophthalmology & Visual Science, 57(11)

ISSN

0146-0404

Authors

Miraftabi, Arezoo
Amini, Navid
Morales, Esteban
et al.

Publication Date

2016-09-13

DOI

10.1167/iovs.16-19648

Peer reviewed

Macular SD-OCT Outcome Measures: Comparison of Local Structure-Function Relationships and Dynamic Range

Arezoo Miraftabi,[1,2] Navid Amini,[1] Esteban Morales,[1] Sharon Henry,[1] Fei Yu,[1,3] Abdolmonem Afifi,[3] Anne L. Coleman,[1] Joseph Caprioli,[1] and Kouros Nouri-Mahdavi[1]

[1]Glaucoma Division, Stein Eye Institute, David Geffen School of Medicine, University of California, Los Angeles, Los Angeles, California, United States
[2]Eye Research Center, Rasoul Akram Hospital, Iran University of Medical Sciences, Tehran, Iran
[3]Department of Biostatistics, Jonathan and Karin Fielding School of Public Health, University of California, Los Angeles, Los Angeles, California, United States

Correspondence: Kouros Nouri-Mahdavi, 100 Stein Plaza, Los Angeles, CA, 90095, USA; nouri-mahdavi@jsei.ucla.edu.

Submitted: March 28, 2016
Accepted: July 14, 2016

Citation: Miraftabi A, Amini N, Morales E, et al. Macular SD-OCT outcome measures: comparison of local structure-function relationships and dynamic range. *Invest Ophthalmol Vis Sci*. 2016;57:4815–4823. DOI:10.1167/iovs.16-19648

Purpose. We tested the hypothesis that the macular ganglion cell layer (GCL) thickness demonstrates a stronger structure-function (SF) relationship and extends the useful range of macular measurements compared with combined macular inner layer or full thickness.

Methods. Ninety-eight glaucomatous eyes and eight normal eyes with macular spectral domain optical coherence tomography (SD-OCT) volume scans and 10-2 visual fields were enrolled. Inner plexiform layer (IPL), GCL, macular retinal nerve fiber layer (mRNFL), ganglion cell-inner plexiform layer (GCIPL), ganglion cell complex (GCC), and full thickness (FT) measurements were calculated for 8×8 arrays of 3° superpixels. Main outcome measures were local structure-function relationships between macular superpixels and corresponding sensitivities on 10-2 fields after adjusting for ganglion cell displacement, dynamic range of measurements, and the change point (total deviation value where macular parameters reached measurement floor).

Results. Median (interquartile range [IQR]) mean deviation was −7.2 (−11.6 to −3.2) dB in glaucoma eyes. Strength of SF relationships was highest for GCIPL, GCL, GCC, and IPL (ρ = 0.635, 0.627, 0.621, and 0.577, respectively; $P \leq 0.046$ for comparisons against GCIPL). Highest SF correlations coincided with the peak of GCL thickness, where the dynamic range was widest for FT (81.1 μm), followed by GCC (65.7 μm), GCIPL (54.9 μm), GCL (35.2 μm), mRNFL (27.5 μm), and IPL (20.9 μm). Change points were similar for all macular parameters (−7.8 to −8.9 dB).

Conclusions. GCIPL, GCL, and GCC demonstrated comparable SF relationships while FT, GCC, and GCIPL had the widest dynamic range. Measurement of GCL did not extend the range of useful structural measurements. Measuring GCL does not provide any advantage for detection of progression with current SD-OCT technology.

Keywords: macular imaging, SD-OCT, dynamic range, structure-function

Identification of glaucoma progression is a pivotal task in day-to-day management of glaucoma, to which various structural and functional measures have been applied. The advent of spectral-domain optical coherence tomography (SD-OCT) has provided the glaucoma research community with a powerful tool for detecting early glaucoma or its progression. Many reports have highlighted the potential role of retinal nerve fiber layer (RNFL),[1,2] although more research is needed to better understand its limitations and the appropriate circumstances for its application. Some recent investigations have demonstrated the utility and added value of macular SD-OCT imaging for detecting glaucoma, but its role remains less well defined with respect to progression.[3–10]

Thanks to development of segmentation algorithms applied to SD-OCT imaging, various inner macular parameters are now available to investigators and clinicians.[3,11,12] These include single layer measurements such as ganglion cell (GCL), inner plexiform (IPL), or retinal nerve fiber layer, combination of inner retinal layers such as the ganglion cell-inner plexiform layer (GCIPL) and the ganglion cell complex (GCC), which includes the combined thickness of the GCIPL and macular RNFL (mRNFL), or the full retinal thickness. The comparative utility of these various thickness parameters for detection of glaucoma progression is unknown. To this aim, the strength of the corresponding structure-function relationships and the comparative dynamic range of these parameters need to be compared. Another issue of interest is the point of change on structure-function plots at which each parameter reaches its measurement floor.

We hypothesized that the macular GCL has a stronger correlation with central visual field sensitivities and may extend the range of useful structural measurements compared with other individual or combined inner retinal layers and may be a better outcome measure for detection of glaucoma progression. To this aim, this study was carried out to compare: (1) localized structure-function relationships between GCL and other macular thickness measurements, (2) the dynamic range of macular structural parameters, and (3) the change point for these parameters (i.e., the approximate threshold sensitivity beyond which the structural measures do not provide much additional information).

Material and Methods

The data for this study were collected from ongoing imaging studies at the Glaucoma Imaging Research Laboratory at Stein Eye Institute, and approved by the institutional review board at the University of California Los Angeles (UCLA). All procedures followed the tenets of the Declaration of Helsinki and respected Health Insurance Portability and Accountability Act regulations. We enrolled 88 perimetric glaucoma eyes (88 patients); 10 eyes (of 10 patients) with preperimetric glaucoma; and 8 normal eyes (of 8 subjects). All eyes had both macular imaging and 10-2 visual fields. Study eyes underwent a complete eye exam, which included best-corrected visual acuity, refraction, corneal pachymetry, slit lamp examination, intraocular pressure measurement with applanation tonometry, gonioscopy, dilated fundus examination, biometry (IOLMaster; Carl Zeiss Meditec, San Leandro, CA, USA), and achromatic visual field testing (SITA standard 24-2 and 10-2 fields with the Humphrey Field Analyzer). Perimetric glaucoma was defined as the presence of glaucomatous optic nerve damage (i.e., vertical cup-to-disc ratio of >0.6, cup to disc asymmetry >0.2, or presence of focal rim thinning or notching) along with a corresponding visual field defect on standard achromatic perimetry (SAP). A visual field defect was considered to be present on 24-2 fields if both of the following criteria were met: (1) glaucoma hemifield test outside normal limits; and (2) four abnormal points with $P < 5\%$ on the pattern deviation plot, both confirmed at least once.[13] An eye was considered to have preperimetric glaucoma if the visual field did not meet the criteria for abnormality but the optic nerve was considered glaucomatous on review of the optic disc photographs by one of the authors (KNM). Patients were also required to meet the following criteria: less than 3 diopters (D) of astigmatism and no significant retinal or neurological disease. The normal subjects had a normal eye exam, open angles, normal appearing optic discs, no RNFL wedge defects, and 24-2 SAP visual fields that did not meet the criteria for an abnormal field.

Imaging and Visual Field Methods

The posterior pole algorithm of the SD-OCT (Spectralis; Heidelberg Engineering, Heidelberg, Germany) was used to obtain 30° × 25° volume scans of the macula centered on the fovea. The algorithm performs 61 horizontal B-scans parallel to the fovea-disc axis, approximately 120 μm apart. Through the automated real time (ART) function of the SD-OCT device (Heidelberg Engineering), each B-scan was repeated between 9 and 11 times to improve image quality. The central 24° × 24° of the measurement cube is segmented by the software and the data are presented in an 8 × 8 array with each superpixel 3° × 3° in width (Fig. 1). The glaucoma module premium edition software (Heidelberg Engineering) performs segmentation of individual retinal layers, and the data are exported as extensible markup language (XML) files. The perimetric glaucoma patients had three consecutive macular volume scans taken during a single session by the same operator. One of the three images was randomly chosen for these patients. The remaining patients had one macular volume scan. Only images with a quality factor of 15 or higher were included. One of the investigators (AM or SH) reviewed all the B-scans and measurement grid positions to verify that the images were centered on the fovea and to check for image artifacts. If more than two B-scans in any individual volume scan were of poor quality or showed poor segmentation, that eye was excluded from analyses. The macular layers (or combination of layers) of interest in this study were as follows: mRNFL, located between the inner limiting membrane (ILM) and the GCL; GCL, the layer between the IPL and mRNFL; IPL: located between the GCL and the inner nuclear layer; GCIPL: the combined thickness of the GCL and IPL; GCC: the combined thickness of mRNFL, GCL, and IPL; and full macular retinal thickness comprising the entire distance between the ILM and the retinal pigment epithelium. The thickness in combinations of layers (GCIPL and GCC) was calculated by adding the thickness of individual layers. The data are presented in right eye format (Fig. 1).

The visual field locations were matched to individual macular superpixels after adjusting for RGC displacement according to Drasdo,[14] and as demonstrated in Figure 2. Only the superpixels and the corresponding visual field (VF) test locations within the central 18° of the macula were further analyzed since the thickness values for the inner retinal layers significantly decrease and reach a plateau beyond this eccentricity.[15,16] Visual field data from the 10-2 fields were exported as XML files and total deviation values extracted. The central 24 superpixels and the corresponding test locations were divided into three circles or subfields according to eccentricity located at a distance of 3.4, 5.6, and 6.8° from the foveal center for circles 1 through 3, respectively (Fig. 2).

Statistical Methods

When both eyes of a subject were eligible, only the right eye was included. Distribution of the numerical and categorical variables was explored with histograms and contingency tables, respectively. Structure-function plots were constructed as bivariate plots with the total deviation at individual test locations on the *x*-axis and various macular thickness parameters (in microns) on the *y*-axis. Nonparametric correlations were estimated (Spearman's ρ) between macular parameters and visual field total deviation values. A bootstrap method was used to compare the Spearman correlation coefficients between various macular parameters and VF data in a pairwise manner.

In this manuscript, the concept of "dynamic range" refers to the difference between the smallest and largest observed thickness values for macular SD-OCT thickness parameters. The following strategy was used to calculate the dynamic range for various macular parameters. A broken stick model was first fit to the structure-function data with the following nonlinear model.

$$y = \begin{cases} a & \text{if } x < C \\ a + b(x - C) & \text{if } x \geq C \end{cases},$$

Where a is the intercept in μm, an estimate of the measurement floor for macular parameters; b is the slope in μm/dB, and C is the threshold sensitivity at the point of change.

The model posits that beyond the change point, the macular thickness reaches its floor level and no change occurs beyond this point. Hence, a flat line was fit to the data below this point and a linear model was fit to the data above the change point and the corresponding slope (b) was calculated. The intercept for the flat linear model was considered the measurement floor. To calculate the ceiling of macular measurements, the 90th percentile measurement for each macular parameter in normal eyes was determined. The dynamic range was considered to be the difference between the intercept for the broken stick model and the 90th percentile normal thickness measure for each macular parameter.[17] All statistical analyses were performed with statistical software, Stata (version 14.0; StataCorp, College Station, TX, USA).

Results

A total of 106 eyes of 106 subjects—including 88 eyes with perimetric glaucoma, 10 eyes with preperimetric glaucoma,

Investigative Ophthalmology & Visual Science

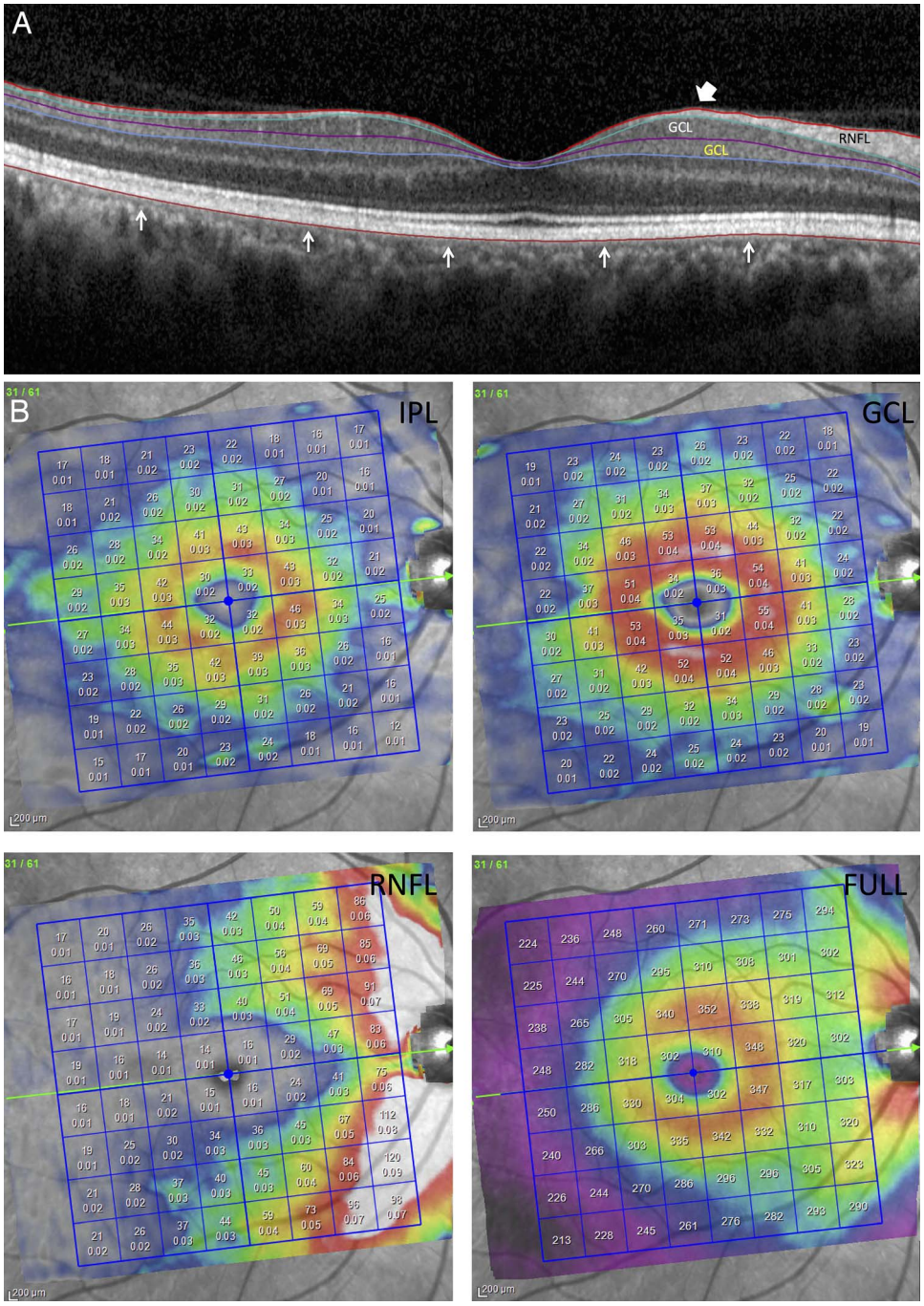

Figure 1. (**A**) An example of inner retinal layer and outer retinal segmentation in a normal subject with the glaucoma premium module edition software (Heidelberg Engineering). *White block arrowhead*: inner limiting membrane; *white arrows* point to the outer border of the retinal pigment epithelium. (**B**) Examples of macular thickness measurements displayed as an 8×8 array of superpixels after segmentation and exporting of the SD-OCT data derived from the posterior pole algorithm of the SD-OCT device (Heidelberg Engineering) in a normal eye.

and eight normal eyes—were included in this study. Table 1 describes the demographic and clinical characteristics of the study sample. The median 10-2 visual field mean deviation was −7.2 dB (IQR, −11.6 to −3.2 dB) in the glaucoma group. The glaucoma patients were older than normal subjects (median [IQR]: 66.0 [59.1–72.5] versus 49.2 [42.9–54.5] years; $P < 0.001$), but had similar axial lengths (median [IQR]: 24.7 [23.9–26.0] versus 24.1 [23.7–24.6] mm; $P = 0.236$).

Because of regional variability in macular topography and thickness, the SD-OCT superpixels and their corresponding test locations were grouped into three subfields (or circles) as a function of the distance from the fovea. Figure 2 describes the three levels of eccentricity for macular superpixels.

Table 2 lists the pairwise correlation coefficients between VF total deviation (TD) values at individual test locations and the corresponding thickness at superpixels for various macular structural measures as a function of eccentricity. When the analyses were repeated after excluding the normal eyes, the results were very similar (data not shown). The strength of SF relationships was highest for GCIPL, GCL, GCC, and IPL (Spearman's $\rho = 0.635$, 0.627, 0.621, and 0.577, respectively) and lowest for mRNFL and FT, regardless of eccentricity. Tables

Investigative Ophthalmology & Visual Science

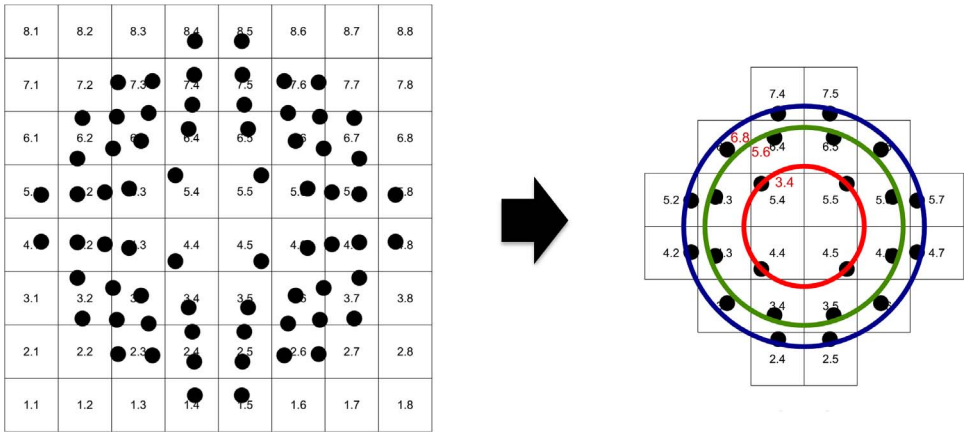

Figure 2. *Left*: matching of the 68 visual field test locations belonging to the 10-2 strategy to the superpixels from the macular SD-OCT image (posterior pole algorithm) after adjusting for retinal ganglion cell displacement in the central macula according to Drasdo.[14] *Right*: the central 24 superpixels and the corresponding test locations are divided into circles according to distance from the fovea. Numbers in red along the circles represent distance in degrees from the fovea.

3 and 4 provide the *P* values for pairwise comparisons of the correlation coefficients for structure-function relationships between various macular parameters and the corresponding TD values with a bootstrap method for all data (Table 3) and as a function of eccentricity (Table 4). Although the SF relationships for GCIPL were significantly larger than all the other parameters (Table 3, $P < 0.046$ for all pairwise comparisons), the magnitude of such differences was not clinically relevant. When categorized according to eccentricity, the results remained unchanged for circles 1 and 2, whereas the magnitude of the Spearman's ρ for the IPL decreased for superpixels furthest from the fovea (circle 3). The highest SF correlations coincided with the peak of the GCL thickness on circle 2 ($\rho = 0.654$, 0.641, 0.669, 0.638, 0.549 for IPL, GCL, GCIPL, GCC, and FT, respectively) except for mRNFL (0.282). For the latter, the highest correlation was observed closer to the fovea on circle 1 ($\rho = 0.458$). Scatter plots showing local SF relationships between various macular parameters and the TD values for the corresponding VF locations confirmed the simple linear model as proposed by Hood and Kardon.[18] Figure 3 demonstrates local structure-function scatter plots for the six macular outcomes of interest versus VF total deviation values for all data regardless of eccentricity. It can be observed that macular measurements display a region of linear relationship with TD values beyond which they reach a floor. These scatter plots are similar in shape to those reported for sectoral RNFL thickness against the corresponding average sectoral MD values as reported by Hood and Kardon.[18]

Figure 4 shows the expected model fits (i.e., expected *y*'s or $\hat{y}$'s, superpixel values here), as predicted by the model versus TD values at corresponding individual test locations, based on the broken stick model, for four inner retinal parameters (IPL, GCL, GCIPL, and GCC) and separately for full thickness measurements against visual field TD values for circle 2 (5.6° eccentricity). The full thickness plot is shown separately given its much higher thickness values. Results for all data regardless of eccentricity and for circles 1 and 3 (3.4° and 6.8° eccentricities) were similar. It can be observed that: (1) the GCL had a higher dynamic range and lower floor compared to IPL; this finding was consistent across all eccentricities (data not shown); (2) the dynamic range of measurements increased as the thickness of the (combined) layers of interest increased (i.e., it was highest for the FT, GCC and GCIPL in that order); (3) the change point where the structural outcomes reached their measurement floor was very consistent among all parameters as follows: –7.8 dB for IPL, –8.4 dB for GCL, –8.9 dB for mRNFL, –8.0 dB for GCIPL, –8.3 dB for GCC, and –7.9 dB for full thickness measurements regardless of eccentricity; and (4) the largest dynamic range measurements belonged to circle 2 superpixels; the measurements for that eccentricity were as follows: FT (81.1 μm), followed by the GCC (65.7 μm), GCIPL (54.9 μm), GCL (35.2 μm), mRNFL (27.5 μm), and IPL (20.9 μm) (Fig. 5).

When the expected macular thickness versus TD plots were inspected as a function of eccentricity, the following two findings were observed: first, the floor level was a function of thickness (i.e., with increasing overall thickness, there was a higher measurement floor: circle 2 measurements had the highest floor followed by circle 3 and 1 measurements); second, the FT measurements actually had the lowest floor of measurement most peripherally: 261.2 μm (95% confidence interval [CI]: 258.7–263.8 μm) for circle 3 versus 288.5 μm (95% CI: 285.2–291.8 μm) for circle 2 versus 288.9 μm (284.8–293.0 μm) for circle 1. Figure 5 demonstrates the scatter plots

Table 1. Demographic and Clinical Characteristics of the Study Subjects

Number (patients/eyes)	Glaucoma (98/98)	Normal (8/8)	*P* Value
Age, y, median (IQR)	66.0 (59.1–72.5)	49.2 (42.9–54.5)	<0.001
Sex (female/male)	59/39	5/3	0.898
Axial length, mm (median [IQR])*	24.7 (23.9–26.0)	24.1 (23.7–24.6)	0.236
24-2 VF mean deviation, dB (median [IQR])**	−6.1 (−10.8 to −3.0)	0.5 (−0.7 to 1.1)	<0.001
10-2 VF mean deviation, dB (median [IQR])	−7.2 dB (−11.6 to −3.2 dB)	0.7 (0.1–1)	<0.001

Mann-Whitney *U* test and χ^2test were used for comparison of numerical and categorical variables, respectively.
* Five glaucoma eyes had missing axial length measurements.
** Six eyes had 24-2 with size *V* and therefore did not have 24-2 mean deviation values.

Table 2. Spearman's Correlation Coefficients for SF Relationships

Eccentricity	IPL	GCL	mRNFL	GCIPL	GCC	FT
Circle 1*	0.571	**0.602**	0.459	**0.601**	**0.608**	0.392
Circle 2†	**0.654**	**0.641**	0.282	**0.669**	**0.638**	0.549
Circle 3‡	0.542	**0.663**	0.416	**0.658**	**0.658**	0.585
All	0.577	**0.627**	0.304	**0.635**	**0.621**	0.513

Values displayed are the Spearman's correlation coefficients between various macular thickness measures and the total deviation values at corresponding test locations for three various eccentricities (first 3 rows), and regardless of eccentricity (*bottom row*). The correlation coefficients above 0.6 have been highlighted in bold font.

* Circle 1 = 3.4° eccentricity.

† Circle 2 = 5.6° eccentricity.

‡ Circle 3 = 6.8° eccentricity.

for the expected macular thickness measurements versus visual field TD values for the FT and GCIPL (as an example), as a function of eccentricity.

Our broken stick model assumes that there is no change in the superpixel thickness for any structural parameter after the threshold sensitivity at the corresponding VF test location reaches the change point. In other words, this model sets the change in *y*-axis (superpixel thickness) to 0 below the change point. We formally tested this hypothesis by performing a linear regression analysis for each of the macular parameters against TD values after excluding superpixels with corresponding TD values greater than the change point for each macular parameter. We hypothesized that if the regression coefficient (i.e., the slope) for these equations was >0 μm/dB in a statistically significant manner for any given macular parameter, that particular parameter could be useful for detection of change in more advanced stages of the disease. We found that only the slope for the full macular thickness, GCIPL, and GCL were significantly positive (regression coefficient = 0.383, 0.077, and 0.076 μm/dB; $P < 0.001$, $P = 0.025$, and $P = 0.001$, respectively). However the R^2 values for all the models were very low ($R^2 = 0.03$, 0.009, and 0.02). This means that a very small amount of variability in the outcome (superpixel thickness) could be explained by the independent variable (TD values at individual test locations).

Discussion

Macular OCT imaging provides a unique opportunity to measure all the components of the RGC/axonal complex in the central retina.[19] This constitutes half of the retinal ganglion cell population critical to human visual function.[15] With the improvements in OCT image quality and more accurate segmentation of these images, individual layers of the macula can be measured.[11,12] There is preliminary evidence that macular measurements may be valuable for identifying disease deterioration in glaucoma. Reproducibility of macular SD-OCT measurements has been demonstrated to be very good to excellent.[3,20–23] We recently found that intrasession variability of various macular measures was excellent at the level of 3 × 3° superpixels.[24] A few studies have explored structure-function relationships between various macular outcome measures and threshold sensitivity in the central 10-2 fields[25,26]; these studies have shown correlations with visual fields that are comparable to those of the RNFL. Sung and colleagues[7] found that full macular thickness measurements showed statistically significant rates of change in patients deteriorating based on stereoscopic disc photographs or visual fields, as compared to RNFL thickness measurements, in a group of advanced glaucoma eyes (average baseline mean deviation: −14.3 dB). Lee et al.[8] found that event analyses based on full macular thickness measures detected a higher percentage of progressing eyes in a group of mostly normal-tension glaucoma eyes.

The strength of structure-function relationships along with the dynamic range of measurements, the visual field sensitivity at the change point, and the variability of the macular measures would facilitate decisions about the utility of macular parameters for measuring glaucoma deterioration. We tested the hypothesis that the GCL can provide a more appropriate structural outcome measure, compared to GCIPL, GCC or full macular thickness, that would have stronger one-to-one structure-function relationships with central 10-2 sensitivity measurements and that could extend the dynamic range of the macular OCT measurements (i.e., would have a change point to the left of other macular parameters). This would have important implications for measuring progression of glaucomatous damage, as the ideal macular outcome for this purpose would be the one with the lowest variability, the widest dynamic range and with a point of change at a lower sensitivity (in dB) along the structure-function plot, as it could potentially extend the utility of structural measures. This approach to comparison of various macular layers of interest has not been previously reported in the literature. We chose the central 18° degrees of the macular measurements since this area of the

Table 3. *P* Values for Pairwise Comparison of Spearman's Correlation Regardless of Eccentricity

Layer	IPL	GCL	mRNFL	GCIPL	GCC	FT
IPL	NA					
GCL	<0.001	NA				
mRNFL	<0.001	<0.001	NA			
GCIPL	<0.001	0.046	<0.001	NA		
GCC	<0.001	0.276	<0.001	0.02	NA	
FT	<0.001	<0.001	<0.001	<0.001	<0.001	NA

Values represent coefficients for SF relationships between various macular thickness measures and the total deviation values at corresponding test locations for all data (i.e., regardless of eccentricity). A bootstrap method was used for estimating the *P* values. NA, not applicable.

Table 4. *P* Values for Pairwise Comparison of Spearman's Correlation Coefficients

Layer	Eccentricity	IPL	GCL	mRNFL	GCIPL	GCC	FT
GCL	Circle 1*	0.057	NA				
	Circle 2†	0.333	NA				
	Circle 3‡	<0.001	NA				
mRNFL	Circle 1*	0.004	<0.001	NA			
	Circle 2†	<0.001	<0.001	NA			
	Circle 3‡	<0.001	<0.001	NA			
GCIPL	Circle 1*	0.008	0.826	<0.001	NA		
	Circle 2†	0.075	<0.001	<0.001	NA		
	Circle 3‡	<0.001	0.494	<0.001	NA		
GCC	Circle 1*	0.056	0.606	<0.001	0.529	NA	
	Circle 2†	0.241	0.736	<0.001	<0.001	NA	
	Circle 3‡	<0.001	0.593	<0.001	0.981	NA	
FT	Circle 1*	<0.001	<0.001	0.124	<0.001	<0.001	NA
	Circle 2†	<0.001	<0.001	0.124	<0.001	<0.001	NA
	Circle 3‡	0.009	<0.001	<0.001	<0.001	<0.001	NA

SF relationships were estimated between various macular thickness measures and the total deviation values at corresponding test locations as a function of eccentricity. A bootstrap method was used for estimating the *P* values. NA, not applicable.

* Circle 1 = 3.4° eccentricity.

† Circle 2 = 5.6° eccentricity.

‡ Circle 3 = 6.8° eccentricity.

Investigative Ophthalmology & Visual Science

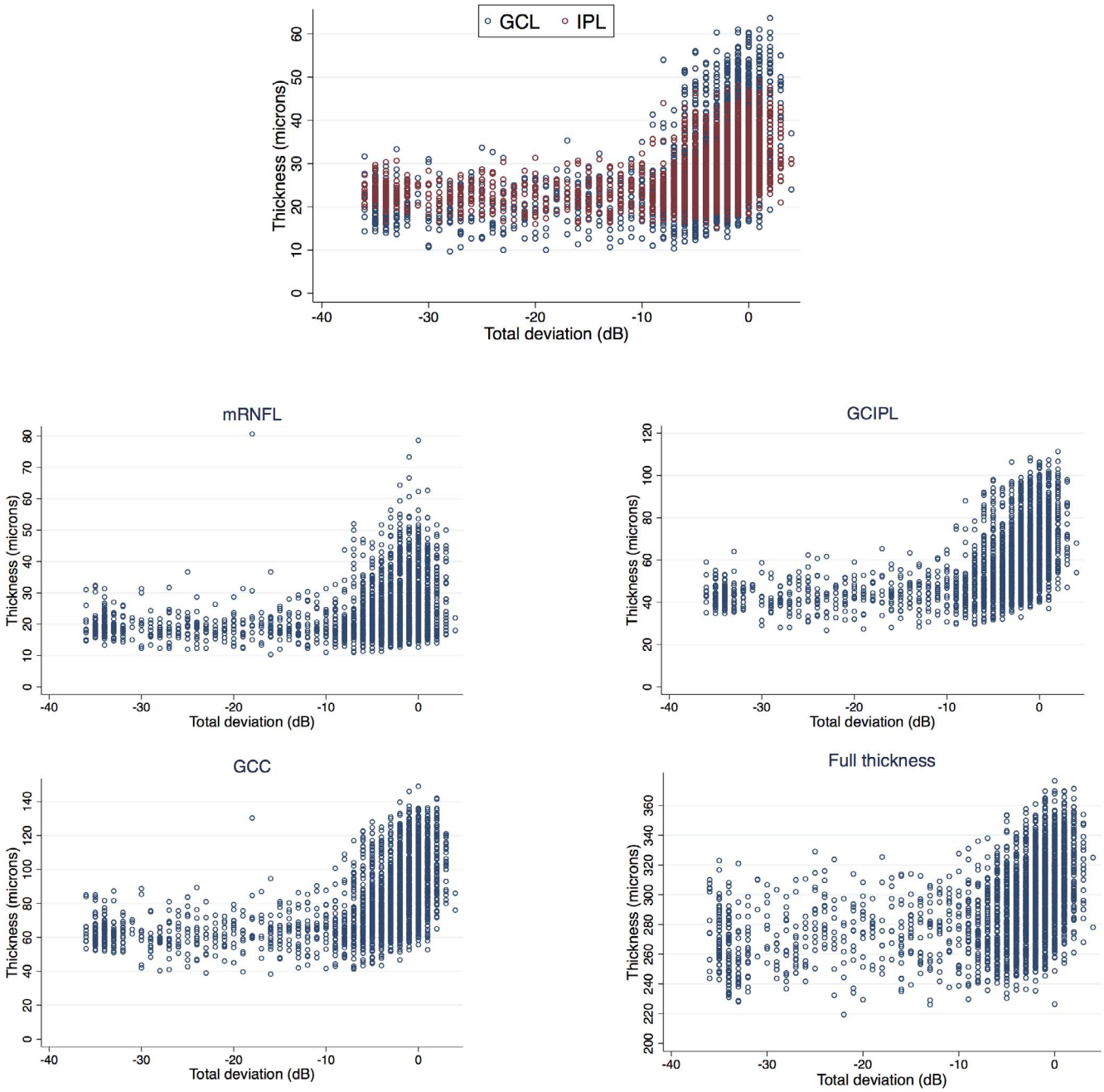

FIGURE 3. Scatter plots showing local SF relationships between various macular parameters and the total deviation values for the corresponding VF locations confirmed the simple linear model as proposed by Hood and Kardon.[18]

macula encompasses most of the RGC mass in the posterior pole.[15,16]

We found that the local structure-function relationships were good and followed the simple linear model described by Hood[27] reaching a plateau after a certain point beyond which they hardly changed. The strength of SF relationships was comparable for GCL, GCIPL, and GCC and was lowest for mRNFL and full macular thickness measurements regardless of eccentricity. Interestingly, the IPL thickness demonstrated as strong a correlation with VF data as those of GCL, GCIPL, and GCC closest to the fovea but its correlation diminished with increasing distance from the fovea. Prior clinical and histologic measurements of the IPL and GCL have demonstrated that the IPL layer thickness reaches a peak at the same distance from the fovea as the GCL but then plateaus until it actually exceeds GCL thickness.[28,29] This may explain the lower correlation of IPL thickness with VF sensitivity measurements farther from the fovea.

Based on a simple linear model, we calculated the change point for all macular parameters beyond which any individual macular parameter would reach its measurement floor. The change point was consistent for all macular parameters although a formal statistical test could not be carried out since these represent single numbers rather than distributions. This finding strongly suggests that GCL thickness measurements did not extend the utility of macular measurements beyond a local

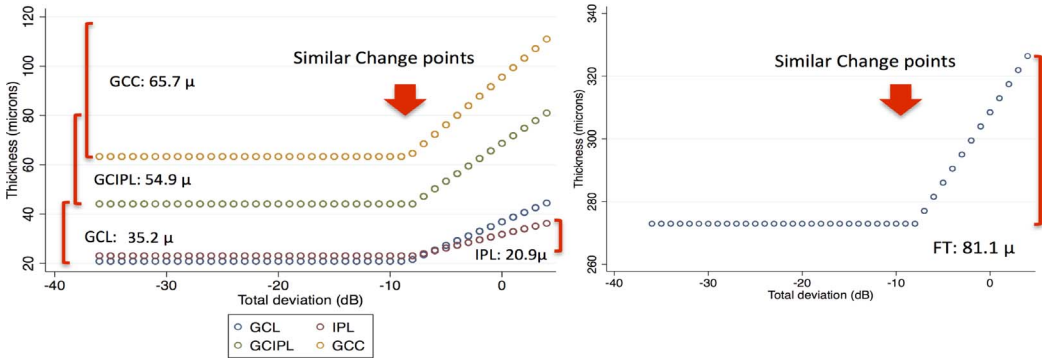

Figure 4. Scatter plots demonstrate the expected model fits (i.e., $\hat{y}$s) for macular thickness parameters at superpixels (y-axis) versus corresponding total deviation values at individual test locations on the x-axis for circle 2 (5.6° eccentricity), based on the broken stick model for (**A**) 4 inner macular parameters (IPL, GCL, GCIPL, and GCC) and (**B**) separately for full thickness measurements. The numbers next to the brackets represent the dynamic range for the data from circle 2 (approximately 5.6° eccentricity) where the dynamic range was highest. The dynamic range was calculated by subtracting the 90-percentile value for the normal group from the intercept of the broken stick model (see Methods, page 2). The full thickness parameters are shown separately because of the much larger thickness range of measurements compared with other parameters.

sensitivity of approximately −10 dB. This is very similar to the change point as reported for the RNFL thickness measurements.[17] However, since the macular RGC axonal complex is less affected until the later stages of glaucoma, such measurements effectively extend the utility of structural outcome measures, notwithstanding that the inherent relationship of macular structural parameters with VF sensitivities is similar to RNFL measures. The other interesting finding of our study was that the dynamic range for the GCC or GCIPL was greater than that for the GCL or IPL; the dynamic range for the GCIPL was almost as large as the sum of the dynamic range for the GCL and IPL. We recently found that the intrasession variability of all macular parameters was quite low and did not exceed ±3 μm for all parameters after excluding a small percentage of outliers.[24] This could mean that GCIPL or GCC measurements may be more suitable for detecting smaller amounts of change over time compared with GCL thickness. In other words, because of the similar variability for all macular outcomes, the magnitude of a step change required to define a significant worsening event is comparable for all such outcomes; hence due to the larger dynamic range of the GCIPL or GCC thickness measurements, they may detect change sooner. This is despite the fact that no macular parameter extends the utility of such measures beyond 10 dB loss of VF sensitivity, or approximately 1 logarithmic unit. A higher dynamic range for GCIPL or GCC could translate into the possibility of detecting change sooner or detecting many more steps of change before the measurement floor is reached. However, this is based on the assumption that steps of change in GCIPL or GCC could be potentially as small as those for GCL. This is an issue that only longitudinal data can adequately address. We must emphasize, however, that our findings should not be understood as a complete lack of utility of macular parameters once the mean deviation for central 10-2 VF has reached a threshold of approximately −10 dB. Rather, macular damage can be more or less localized in glaucoma and while in some areas of the macula, the RGC/axonal complex may have reached its measurement floor, in other areas adequate thickness may be preserved that could be valuable to detect worsening. This issue needs to be further investigated.

Our statistical approach forced all parameters to hit a measurement floor and assumed a zero slope for the measurements beyond this change point. We formally tested this assumption by carrying out linear regression analyses on data beyond the change point. A statistically significant and positive slope was found only for GCL, GCIPL, and FT measurements. However, the amount of variability in the outcome explained by the model was very low ($R^2 = 0.02$, 0.009, and 0.03, respectively). One caveat, however, is that the conclusions of this study are based on cross-sectional data and hence, the large interindividual variability of structural measurements could result in a lower performance of these parameters than that of same parameters from truly longitudinal data. Therefore, macular structural measurements, especially FT measures, might be helpful for monitoring disease

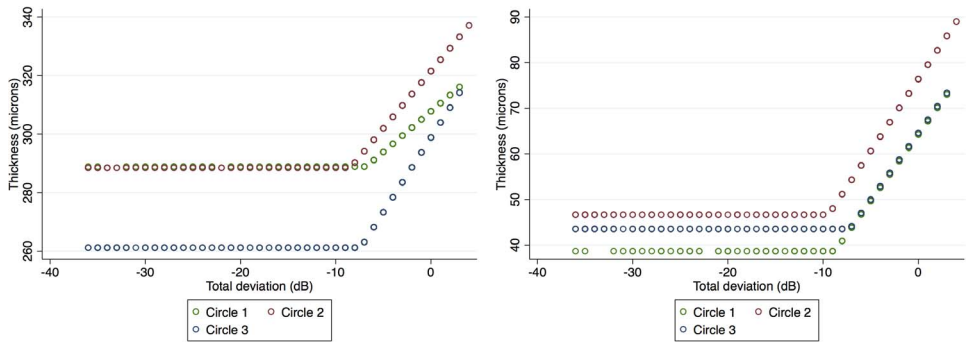

Figure 5. Scatter plots for the expected model fits (i.e., $\hat{y}$s) for full thickness (left) and ganglion cell/inner plexiform layer measurements at inner 24 superpixels versus corresponding total deviation values, based on the broken stick model as a function of eccentricity.

Investigative Ophthalmology & Visual Science

progression in areas of the macula where most other inner retinal measurements have reached their floor. We found that the measurement's floor level was significantly lower for the FT measurements in circle 3. There is no clear explanation for this finding; however, this may be related to changes in the outer retinal layer thickness since this finding was not observed with any of the inner retinal parameters. This will need to be explored in longitudinal studies.

The findings of our study should be interpreted within the context of its limitations. The control group was a convenience sample of normal subjects who were on average younger than the glaucoma group. However, given the fact that all of the outcome comparisons were within-group comparisons, the age discrepancy or any other measured or unmeasured confounding variables are unlikely to have significantly affected the results. The study sample included eyes with a range of glaucoma severity and the MD for the most advanced eye was −24.3 dB. This might have affected our results since there were not many eyes with end-stage glaucoma in this group. Regardless, we expect that at some point along the way, with worsening severity of the disease, structural measures cease to be of any help and functional outcomes become the only option for monitoring glaucoma. The point at which this happens may vary among patients and is worth further exploration. One could argue that the dynamic range of macular measurements as estimated in this study might represent an overestimation. Although this is a possibility, because the comparisons are between pairs of measurements, we do not believe that the method used for estimating the dynamic range would have significantly affected the relative performance of various macular parameters. Macular diseases become more prevalent with age and hence, the utility of macular parameters diminishes with aging. However, no study has yet explored the influence of milder degrees of outer retinal pathology such as small to large drusen on the inner macular thickness measurements. The fair correlation between the mRNFL and individual visual field sensitivity measurements is partly an artifact of the way we analyzed the data. The thickness measurements of mRNFL in localized areas of the macula do not necessarily represent the sensitivity of the underlying RGCs given the anatomy of the RNFL. Therefore, it was expected that such mRNFL thickness measurements would not be as highly correlated to VF sensitivity.

In summary, we found that measuring the ganglion cell layer did not result in a stronger structure-function relationship with central visual field sensitivity measurements compared with GCIPL or GCC thickness; also, there was no evidence that GCL measurements extended the dynamic range of structural measures. Given the similar reproducibility for all individual or combined inner macular layers, and the less demanding segmentation of the GCIPL or GCC layers, the latter parameters currently provide the best compromise for monitoring the health of the RGC/axonal complex in glaucoma patients.

Acknowledgments

Presented as a poster at the annual meeting of the American Glaucoma Society, March 3–6, 2016, Fort Lauderdale, FL, United States and as an oral presentation at the annual meeting of the Association for Research in Vision and Ophthalmology, May 1–5, 2016, Seattle, WA, United States.

Supported by a Mid-Career Clinician-Scientist Grant from the American Glaucoma Society (KNM); a National Institutes of Health Mentored Patient-Oriented Research Career Development Award (5K23EY022659; KNM); and an unrestricted Departmental Grant from Research To Prevent Blindness.

Disclosure: **A. Miraftabi**, None; **N. Amini**, None; **E. Morales**, None; **S. Henry**, None; **F. Yu**, None; **A. Afifi**, None; **A.L. Coleman**, None; **J. Caprioli**, Allergan (C); **K. Nouri-Mahdavi**, Allergan (C), Heidelberg Engineering (R)

References

1. Leung CK. Diagnosing glaucoma progression with optical coherence tomography. *Curr Opin Ophthalmol*. 2014;25:104–111.
2. Bussel II, Wollstein G, Schuman JS. OCT for glaucoma diagnosis, screening and detection of glaucoma progression. *Br J Ophthalmol*. 2014;98(suppl 2):ii15–19.
3. Tan O, Chopra V, Lu AT, et al. Detection of macular ganglion cell loss in glaucoma by Fourier-domain optical coherence tomography. *Ophthalmology*. 2009;116:2305–2314.
4. Mwanza JC, Oakley JD, Budenz DL, Chang RT, Knight OJ, Feuer WJ. Macular ganglion cell-inner plexiform layer: automated detection and thickness reproducibility with spectral domain-optical coherence tomography in glaucoma. *Invest Ophthalmol Vis Sci*. 2011;52:8323–8329.
5. Nouri-Mahdavi K, Nowroozizadeh S, Nassiri N, et al. Macular ganglion cell/inner plexiform layer measurements by spectral domain optical coherence tomography for detection of early glaucoma and comparison to retinal nerve fiber layer measurements. *Am J Ophthalmol*. 2013;156:1297–1307.
6. Na JH, Kook MS, Lee Y, Baek S. Structure-function relationship of the macular visual field sensitivity and the ganglion cell complex thickness in glaucoma. *Invest Ophthalmol Vis Sci*. 2012;53:5044–5051.
7. Sung KR, Sun JH, Na JH, Lee JY, Lee Y. Progression detection capability of macular thickness in advanced glaucomatous eyes. *Ophthalmology*. 2012;119:308–313.
8. Lee KS, Lee JR, Na JH, Kook MS. Usefulness of macular thickness derived from spectral-domain optical coherence tomography in the detection of glaucoma progression. *Invest Ophthalmol Vis Sci*. 2013;54:1941–1949.
9. Na JH, Sung KR, Lee JR, et al. Detection of glaucomatous progression by spectral-domain optical coherence tomography. *Ophthalmology*. 2013;120:1388–1395.
10. Suda K, Hangai M, Akagi T, et al. Comparison of longitudinal changes in functional and structural measures for evaluating progression of glaucomatous optic neuropathy. *Invest Ophthalmol Vis Sci*. 2015;56:5477–5484.
11. Ooto S, Hangai M, Tomidokoro A, et al. Effects of age, sex, and axial length on the three-dimensional profile of normal macular layer structures. *Invest Ophthalmol Vis Sci*. 2011;52:8769–8779.
12. Raza AS, Hood DC. Evaluation of a method for estimating retinal ganglion cell counts using visual fields and optical coherence tomography. *Invest Ophthalmol Vis Sci*. 2015;56:2254–2268.
13. Johnson CA, Sample PA, Cioffi GA, Liebmann JR, Weinreb RN. Structure and function evaluation (SAFE): I. criteria for glaucomatous visual field loss using standard automated perimetry (SAP) and short wavelength automated perimetry (SWAP). *Am J Ophthalmol*. 2002;134:177–185.
14. Drasdo N, Millican CL, Katholi CR, Curcio CA. The length of Henle fibers in the human retina and a model of ganglion receptive field density in the visual field. *Vision Res*. 2007;47:2901–2911.
15. Curcio CA, Allen KA. Topography of ganglion cells in human retina. *J Comp Neurol*. 1990;300:5–25.
16. Mwanza JC, Durbin MK, Budenz DL, et al. Profile and predictors of normal ganglion cell-inner plexiform layer thickness measured with frequency-domain optical coherence tomography. *Invest Ophthalmol Vis Sci*. 2011;52:7872–7879.
17. Mwanza JC, Kim HY, Budenz DL, et al. Residual and dynamic range of retinal nerve fiber layer thickness in glaucoma:

Comparison of three OCT platforms. *Invest Ophthalmol Vis Sci*. 2015;56:6344–6351.

18. Hood DC, Kardon RH. A framework for comparing structural and functional measures of glaucomatous damage. *Prog Retin Eye Res*. 2007;26:688–710.
19. Bogunović H, Kwon YH, Rashid A, et al. Relationships of retinal structure and Humphrey 24-2 visual field thresholds in patients with glaucoma. *Invest Ophthalmol Vis Sci*. 2015;56: 259–271.
20. Garas A, Vargha P, Hollo G. Reproducibility of retinal nerve fiber layer and macular thickness measurement with the RTVue-100 optical coherence tomograph. *Ophthalmology*. 2010;117:738–746.
21. Ishikawa H, Stein DM, Wollstein G, Beaton S, Fujimoto JG, Schuman JS. Macular segmentation with optical coherence tomography. *Invest Ophthalmol Vis Sci*. 2005;46:2012–2017.
22. Matlach J, Wagner M, Malzahn U, Göbel W. Repeatability of peripapillary retinal nerve fiber layer and inner retinal thickness among two spectral domain optical coherence tomography devices. *Invest Ophthalmol Vis Sci*. 2014;55: 6536–6546.
23. Kim KE, Yoo BW, Jeoung JW, Park KH. Long-term reproducibility of macular ganglion cell analysis in clinically stable glaucoma patients. *Invest Ophthalmol Vis Sci*. 2015;56:4857–4764.
24. Miraftabi A, Amini A, Gornbein J, et al. Local Variability of Macular Thickness Measurements with SD-OCT and Influencing Factors. *Trans Vis Sci Tech*. 2016;5(4):5.
25. Ohkubo S, Higashide T, Udagawa S, et al. Focal relationship between structure and function within the central 10 degrees in glaucoma. *Invest Ophthalmol Vis Sci*. 2014;55:5269–5277.
26. Rao HL, Januwada M, Hussain RS, et al. Comparing the structure-function relationship at the macula with standard automated perimetry and microperimetry. *Invest Ophthalmol Vis Sci*. 2015;56:8063–8068.
27. Hood DC, Anderson SC, Wall M, Kardon RH. Structure versus function in glaucoma: an application of a linear model. *Invest Ophthalmol Vis Sci*. 2007;48:3662–3668.
28. Curcio CA, Messinger JD, Sloan KR, Mitra A, McGwin G, Spaide RF. Human chorioretinal layer thicknesses measured in macula-wide, high-resolution histologic sections. *Invest Ophthalmol Vis Sci*. 2011;52:3943–3954.
29. Moura AL, Raza AS, Lazow MA, De Moraes CG, Hood DC. Retinal ganglion cell and inner plexiform layer thickness measurements in regions of severe visual field sensitivity loss in patients with glaucoma. *Eye (Lond)*. 2012;26:1188–1193.

Investigative Ophthalmology & Visual Science